Progress In Electromagnetics Research, PIER 80, 29–44, 2008

FAST ANALYSIS OF ANTENNA MOUNTED ON ELECTRICALLY LARGE COMPOSITE OBJECTS

J. Yuan † **and Y. Qiu**

EMC Laboratory of school of electromechanical engineering
Xidian University
Xi'an, Shaanxi 710071, P. R. China

J. L. Guo, Y. L. Zou, and Q. Z. Liu

National Key Laboratory of Antennas and Microwave Technology
Xidian University
Xi'an, Shaanxi 710071, P. R. China

Abstract—Several characteristics of the wire antenna on electrically large composite body are analyzed by an adaptive multilevel fast multipole algorithm (MLFMA). Adaptive MLFMA is applied to the boundary integration of the analysis model. With the basis functions and testing functions expanded with Dirac functions on different position, the calculation of impedance integration can be simplified and all the translation process can be calculated by fast Fourier transformation (FFT). Good agreement between the computed and measured results of antenna characters is obtained.

1. INTRODUCTION

In engineering the antenna characteristics are usually obtained in laboratory by experiment and then the antenna is installed on carrier directly. In fact the antenna characteristics such as radiation pattern, input impedance and gain are always affected by the carrier body, which will influence the work performance and electromagnetic compatibility of antenna system, that is to say, the carrier body becomes one part of the antenna system and the new system has new characteristics. For the profile complexity, large size and material

† Also with National Key Laboratory of Antennas and Microwave Technology, Xidian University, Xi'an 710071, P. R. China

characteristics of the carrier, it is always very difficult to obtain antenna characteristics by experiment after installation. So, the simulation is usually an effective method.

In this paper the characteristics of antennae on electrically large composite object is analyzed by an adaptive MLFMA. The boundary-integral equations of composite object are established first. However, the use of the conventional boundary-integral method for integral equations always results in full matrices. MLFMA [1, 2] is always applied to the integral equation to significantly reduce the memory requirement and computational time. But some targets are very electrically large and the electromagnetic simulation of these targets can not be solved by traditional method on single computer in engineering, so the performance of traditional MLFMA should be improved for electrically larger problems.

In the adaptive MLFMA presented, by expanding the basis functions and testing functions with Dirac functions on different position, the calculation of impedance integration can be simplified and all the translation operation can be calculated by FFT and the CPU time and computer memory are greatly reduced.

2. ANALYSIS MODEL AND FORMULATIONS

We assume there is an antenna on a composite body illustrated in Fig. 1. The composite body consists of metallic and dielectric medium. In this paper, antenna is also seen as metal. The integral equations on the surface of composite object should be established first. In Fig. 1, the metallic medium is in volume V_1 and the surface of V_1 is S_1. The

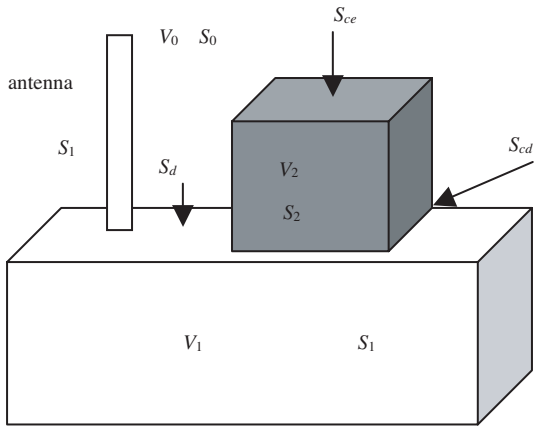

Figure 1. An antenna on a composite object.

dielectric medium is in volume V_2 and the surface of V_2 is S_2. Volume V_0 is free space and S_0 is the boundary surface of free space and the composite object. S_{cd} denotes the boundary surface of V_1 and V_2, S_{ce} denotes the boundary surface of V_0 and V_2 and S_d denotes the boundary surface of V_0 and V_1, so $S_0 = S_{ce} + S_d$ and $S_1 = S_{cd} + S_d$.

The equivalent electric current and magnetic current on $S_i (i = 0, 1, 2)$ are

$$\boldsymbol{J}_i = \hat{n}_i \times \boldsymbol{H}_i \ (i = 0, 1, 2) \ (\text{on } S_i) \tag{1}$$

$$\boldsymbol{M}_i = \boldsymbol{E}_i \times \hat{n}_i \ (i = 0, 1, 2) \ (\text{on } S_i) \tag{2}$$

where $\boldsymbol{E}_i$ and $\boldsymbol{H}_i$ are the total electromagnetic field in volume V_i. In volume V_0 the total electromagnetic field is

$$\theta(\boldsymbol{r})\boldsymbol{E}_0(\boldsymbol{r}) = \boldsymbol{E}^i - L_0\boldsymbol{J}_0(\boldsymbol{r}') + K_0\boldsymbol{M}_0(\boldsymbol{r}') \tag{3}$$

$$\theta(\boldsymbol{r})\boldsymbol{H}_0(\boldsymbol{r}) = \boldsymbol{H}^i - K_0\boldsymbol{J}_0(\boldsymbol{r}') - \frac{1}{\eta_0^2}L_0\boldsymbol{M}_0(\boldsymbol{r}') \tag{4}$$

where

$$\theta(\boldsymbol{r}) = \begin{cases} 1, & \boldsymbol{r} \in V_i, & i = 0, 1 \\ 1/2, & \boldsymbol{r} \in S_i, & i = 0, 1 \\ 0, & \boldsymbol{r} \notin V_i, \quad \boldsymbol{r} \notin S_i, & i = 0, 1 \end{cases} \tag{5}$$

L_i and K_i are integration operators and G_i is the Green's function in free space

$$L_i\boldsymbol{Z}(\boldsymbol{r}') = j\omega\mu_i \int\limits_S \left[\boldsymbol{Z}(\boldsymbol{r}') - \frac{1}{\omega^2\mu_i\varepsilon_i}\nabla\nabla' \cdot \boldsymbol{Z}(\boldsymbol{r}')\right] \cdot G_i \mathrm{d}s' \tag{6}$$

$$K_i\boldsymbol{Z}(\boldsymbol{r}') = -\int\limits_S \boldsymbol{Z}(\boldsymbol{r}') \times \nabla G_i \mathrm{d}s \tag{7}$$

$$G_i = \frac{e^{-jk_i|\boldsymbol{r}-\boldsymbol{r}'|}}{4\pi\,|\boldsymbol{r}-\boldsymbol{r}'|} \tag{8}$$

where $k_i = \omega\sqrt{\mu_i\varepsilon_i}$ and $\eta_i = \sqrt{\frac{\mu_i}{\varepsilon_i}}$. We applied impedance boundary condition (IBC) to surface S_{cd} and S_{ce}

$$\boldsymbol{E}_1 - (\hat{n}_1 \cdot \boldsymbol{E}_1)\hat{n}_1 = \eta_{cd}\eta_0(\hat{n}_1 \times \boldsymbol{H}_1) \tag{9}$$

$$\boldsymbol{E}_0 - (\hat{n}_0 \cdot \boldsymbol{E}_0)\hat{n}_0 = \eta_{ce}\eta_0(\hat{n}_0 \times \boldsymbol{H}_0) \tag{10}$$

where η_{cd} and η_{ce} are the normalized surface impedance of S_{cd} and S_{ce}. On surface S_d the tangential components of electromagnetic field are

continuous

$$\boldsymbol{E}_1|_{\tan} = \boldsymbol{E}_0|_{\tan} \text{ (on } S_d) \tag{11}$$

$$\hat{n}_1 \times \boldsymbol{H}_1 = -\hat{n}_0 \times \boldsymbol{H}_0 \text{ (on } S_d) \tag{12}$$

The combined electric field integration and magnetic field integration (CFIE) on S_{cd} and S_{ce} can be obtained by (9) and (10),

$$\frac{\alpha}{\eta_0}\{\boldsymbol{E}_1 - (\hat{n}_1 \cdot \boldsymbol{E}_1)\hat{n}_1\} = \beta\{\eta_{cd}\hat{n}_1 \times \boldsymbol{H}_1\} \text{ (on } S_{cd}) \tag{13}$$

$$\frac{\alpha}{\eta_0}\{\boldsymbol{E}_0 - (\hat{n}_0 \cdot \boldsymbol{E}_0)\hat{n}_0\} = \beta\{\eta_{ce}\hat{n}_0 \times \boldsymbol{H}_0\} \text{ (on } S_{ce}) \tag{14}$$

with (3), (4), (13) and (14), we can obtain the CFIE on S_{cd}, S_{ce} and S_d .

$$\begin{aligned}&\frac{\alpha}{\eta_0}\left\{L_{1cd}\boldsymbol{J}_{cd} - \eta_{cd}\eta_0\left[K_{1cd}(\boldsymbol{J}_{cd} \times \hat{n}_1) + \frac{1}{2}\boldsymbol{J}_{cd}\right] - L_{1d}\boldsymbol{J}_d + K_{1d}\boldsymbol{M}_d\right\}_{\tan}\\ &-\beta\eta_{cd}\left\{\frac{1}{2}\boldsymbol{J}_{cd} + \hat{n}_1 \times \left[K_{1cd}\boldsymbol{J}_{cd} + L_{1cd}\eta_{cd}\eta_0(\boldsymbol{J}_{cd} \times \hat{n}_1)/\eta_1^2 - K_{1d}\boldsymbol{J}_d\right.\right.\\ &\left.\left.-L_{1d}\boldsymbol{M}_d/\eta_1^2\right]\right\} = 0\end{aligned} \tag{15}$$

$$\begin{aligned}&\frac{\alpha}{\eta_0}\left\{L_{0ce}\boldsymbol{J}_{ce} - \eta_{ce}\eta_0\left[K_{0ce}(\boldsymbol{J}_{ce} \times \hat{n}_0) + \frac{1}{2}\boldsymbol{J}_{ce}\right] - L_{0d}\boldsymbol{J}_d + K_{0d}\boldsymbol{M}_d\right\}_{\tan}\\ &-\beta\eta_{ce}\left\{\frac{1}{2}\boldsymbol{J}_{ce} + \hat{n}_0 \times \left[K_{0ce}\boldsymbol{J}_{ce} + L_{0ce}\eta_{ce}\eta_0(\boldsymbol{J}_{ce} \times \hat{n}_0)/\eta_0^2 - K_{0d}\boldsymbol{J}_d\right.\right.\\ &\left.\left.-L_{0d}\boldsymbol{M}_d/\eta_0^2\right]\right\} = \frac{1}{\eta_0}\left\{\alpha\boldsymbol{E}^i_{\tan} - \beta\eta_{ce}\eta_0\hat{n}_0 \times \boldsymbol{H}_i\right\}\end{aligned} \tag{16}$$

$$\begin{aligned}&\frac{1}{\eta_0}\{-L_{1cd}\boldsymbol{J}_{cd} + K_{1cd}\eta_{cd}\eta_0(\boldsymbol{J}_{cd} \times \hat{n}_1) + L_{0ce}\boldsymbol{J}_{ce} - K_{0ce}\eta_{ce}\eta_0(\boldsymbol{J}_{ce} \times \hat{n}_0)\\ &+(L_{1d} + L_{0d})\boldsymbol{J}_d - (K_{1d} + K_{0d})\boldsymbol{M}_d\}_{\tan} = \frac{1}{\eta_0}\boldsymbol{E}^i_{\tan}\end{aligned} \tag{17}$$

$$\begin{aligned}&\hat{n}_0 \times \{-K_{1cd}\boldsymbol{J}_{cd} - L_{1cd}\eta_{cd}\eta_0(\boldsymbol{J}_{cd} \times \hat{n}_1) + K_{0ce}\boldsymbol{J}_{ce} + L_{0ce}\eta_{ce}\eta_0(\boldsymbol{J}_{ce} \times \hat{n}_0)\\ &+(K_{1d} + K_{0d})\boldsymbol{J}_d + \left(\frac{1}{\eta_1^2}L_{1d} + \frac{1}{\eta_0^2}L_{0d}\right)\boldsymbol{M}_d\Big\} = \hat{n}_0 \times \boldsymbol{H}_i\end{aligned} \tag{18}$$

Solving Equations (15)–(18), we can obtain the electric currents and magnetic currents $\boldsymbol{J}_{cd}$, $\boldsymbol{J}_{ce}$, $\boldsymbol{J}_d$ and $\boldsymbol{M}_d$. MLFMA is very suitable

for solving integral equations, in MLFMA Green's function G_i can be written as

$$G_i = \frac{e^{-jk_i|\boldsymbol{r}-\boldsymbol{r}'|}}{4\pi\,|\boldsymbol{r}-\boldsymbol{r}'|} \approx \frac{-jk}{16\pi^2}\int \mathrm{d}^2\hat{k}e^{-j\boldsymbol{k}\cdot(\boldsymbol{r}_{jm}-\boldsymbol{r}_{im'})}T_L(\boldsymbol{k}\cdot\boldsymbol{r}_{mm'}) \tag{19}$$

where

$$T_L = \sum_{l=0}^{L}(-j)^l(2l+1)h_l^{(2)}(kr_{m'})p_l\left(\hat{k}\cdot\hat{r}_{mm'}\right) \tag{20}$$

is the translation operator of MLFMA. The gradient expression of G_i is

$$\nabla G_i = -j\boldsymbol{k}\left[\frac{-jk}{16\pi^2}\int \mathrm{d}^2\hat{k}e^{-j\boldsymbol{k}\cdot(\boldsymbol{r}_{jm}-\boldsymbol{r}_{im'})}T_L(\boldsymbol{k}\cdot\boldsymbol{r}_{mm'})\right] \tag{21}$$

Applying the vector basis function $\boldsymbol{f}_i$ and combining (6), (7), (19) and (21), we can obtain the multipole expansion expressions of L and K operators

$$L\boldsymbol{Z}(\boldsymbol{r}') = \frac{\omega\mu k}{16\pi^2}\int \mathrm{d}s\int \mathrm{d}s' e^{-j\boldsymbol{k}\cdot(\boldsymbol{r}_{jm}-\boldsymbol{r}_{im'})}T_L(\boldsymbol{k}\cdot\boldsymbol{r}_{mm'})\left(\overline{\overline{\boldsymbol{I}}}-\hat{k}\hat{k}\right)\cdot\boldsymbol{f}_i(\boldsymbol{r}')a_i \tag{22}$$

$$K\boldsymbol{Z}(\boldsymbol{r}') = \frac{k^2}{16\pi^2}\int \mathrm{d}s\int \mathrm{d}s' e^{-j\boldsymbol{k}\cdot(\boldsymbol{r}_{jm}-\boldsymbol{r}_{im'})}T_L(\boldsymbol{k}\cdot\boldsymbol{r}_{mm'})\left(\boldsymbol{f}_i(\boldsymbol{r}')\times\hat{k}\right)a_i \tag{23}$$

where a_i is the expansion coefficients of electric current and magnetic current. Substituting (22) and (23) into (15)–(18), the aggregation operator and disaggregation operator of MLFMA can be written as

$$\boldsymbol{V}_{sm'i}(\hat{k}) = \int_{f_i}(\boldsymbol{r}')e^{-j\hat{k}\cdot\hat{r}_{im'}}\mathrm{d}s' \tag{24}$$

$$\begin{aligned} V_{fmj} \;=\; & \sum_{m=1}^{M}\alpha_m\int \mathrm{d}s e^{-j\hat{k}\cdot\hat{r}_{jm}}\left(\overline{\overline{I}}-\hat{k}\hat{k}\right)\cdot f_j(\boldsymbol{r}) \\ & +\sum_{n=1}^{N}\beta_n\int \mathrm{d}s e^{-j\hat{k}\cdot\hat{r}_{jm}}\left(f_j(\boldsymbol{r})\times\hat{k}\right) \end{aligned} \tag{25}$$

in (25), α_m and β_n are the coefficients of L_i and K_i operators , M and N are the number of L_i and K_i operators in Equations (15)–(18).

In traditional MLFMA there are three computation processes that consume CPU time and memory: 1) the computation of impedance

integration; 2) the computation of translation process; and 3) the computation of translation factor T_L.

While computing the integral formulation of the near-field interaction in MLFMA, the basis function $\boldsymbol{f}_i$ and testing function $\boldsymbol{f}_j$ can be approximated as linear combinations of Dirac delta functions on the Gaussian integration points

$$g \approx \tilde{g} = \sum_{s=1}^{I_G} p_{sr'} \delta_s^3 (r - r') \quad g \in \{f_x, f_y, f_z\} \tag{26}$$

We let

$$\int (x - x_{j0})(y - y_{j0})(z - z_{j0}) \times \left[g - \sum_{s=1}^{I_G} p_{sr'} \delta_s^3 (r - r') \right] ds = 0 \tag{27}$$

the point (x_{j0}, y_{j0}, z_{j0}) is at the center of $\boldsymbol{f}_i$ or $\boldsymbol{f}_j$. According to (27), a matrix equation of the expansion coefficient $p_{sr'}$ can be obtained and then $p_{sr'}$ can be derived.

$$\sum \boldsymbol{W}_{I_G r'} p_{sr'} = O_{sI_G} \tag{28}$$

where

$$O_{sI_G} = \int (x - x_{j0})(y - y_{j0})(z - z_{j0}) g_j ds \tag{29}$$

$$\boldsymbol{W}_{I_G r'} = \left(x' - x_{j0}\right) \left(y' - y_{j0}\right)(z' - z_{j0}) \tag{30}$$

Substituting (26) into the near-field interaction integral formulations, we can see that the calculation speed and precision of integral formulations are controlled by the Gaussian integral coefficient w_s and the expansion coefficient $p_{sr'}$ of basis and testing functions.

$$\int \boldsymbol{f}_i(\boldsymbol{r}') \cdot \boldsymbol{f}_j(\boldsymbol{r}) \cdot \overline{\overline{G}}(\boldsymbol{r}, \boldsymbol{r}') ds = \sum_{s_i=1}^{I_G} \sum_{s_j=1}^{I_{G'}} w_{s_i} p_{s_i} w_{s_j} p_{s_j} G \tag{31}$$

For computing $\boldsymbol{V}_{fmj}$, testing function $\boldsymbol{f}_j$ can be approximated in the same way as in the near-field integral.

Through the expansion, the integral computation of near-field interaction and $\boldsymbol{V}_{fmj}$ can be simplified. The speed and precision can be controlled also. For an arbitrarily shaped body, if the following rules are used, the calculation error of integral computation can be controlled within 1%.

1) For the surface whose curvature is discontinuous, if the distance between the triangle elements center and curvature center less than 0.5λ, where λ is wave length, then the normal number of Gaussian integral points should be employed.
2) For the surface whose curvature is continuous and finite, such as sphere surface and cylinder surface, the number of Gaussian integral points employed is less than 0.7 times of normal number.
3) For the surface whose curvature is continuous and infinite, for example plane surface, the number of Gaussian integral points employed is less than 0.6 times of normal number.

While computing $\boldsymbol{V}_{sm'i}$, basis function $\boldsymbol{f}_i$ can be approximated as linear combinations of Dirac delta functions on the centers of grids grouped uniformly in MLFMA (Fig. 2).

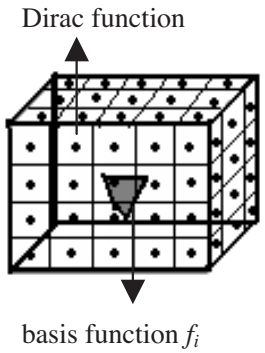

Figure 2. Expansion of basis function f_i.

$$g_i \approx \widetilde{g}_i = \sum_{r' \in C_i} \beta_{ir'} \delta^3(r - r') \quad g_i \in \{f_{ix}, f_{iy}, f_{iz}\} \tag{32}$$

where C_i is the number of grid centers around basis $\boldsymbol{f}_i$.

We let

$$\int (x - x_{i0})(y - y_{i0})(z - z_{i0}) \times \left[g_i - \sum_{s=1}^{I_G} \beta_{ir'} \delta^3(r - r') \right] ds = 0 \tag{33}$$

the point $(x_{i0},\ y_{i0},\ z_{i0})$ is at the center of $\boldsymbol{f}_i$. According to (33), a matrix equation of the the expansion coefficient $\beta_{ir'}$ can be obtain.ed and then $\beta_{ir'}$ can be derived.

$$\sum \boldsymbol{W}_{C_i r'} \beta_{ir'} = O_{iC_i} \tag{34}$$

where

$$O_{iC_i} = \int (x - x_{i0})(y - y_{i0})(z - z_{i0}) g_i ds \tag{35}$$

$$\boldsymbol{W}_{C_i r'} = (x' - x_{i0})(y' - y_{i0})(z' - z_{i0}) \tag{36}$$

Through this expansion operation, the integral computation of $\boldsymbol{V}_{sm'i}$ can be simplified like $\boldsymbol{V}_{fmj}$ and near-field interaction that we have discussed above and there is another advantage by using this expansion. We notice that basis function $\boldsymbol{f}_i$ is mapped to the grid centers around $\boldsymbol{f}_i$ through this expansion and the grids around $\boldsymbol{f}_i$ are filled by Dirac functions, then the translation formulation of MLFMA is a discrete circle convolution and can be calculated by FFT.

$$\sum_{m' \in G_{m'}} T_L \boldsymbol{S}_{m'} = FFT^{-1}\{FFT([\boldsymbol{S}_{m'}]) \times FFT([T_L])\} \tag{37}$$

where

$$\boldsymbol{S}_{m'}\left(\hat{k}\right) = \sum_i \boldsymbol{V}_{sm'i}\left(\hat{k}\right) \boldsymbol{a}_i, \tag{38}$$

In practice we can enclose every parts of the target by multiple cubes (Fig. 3). Each cube is divided by grids in uniform size on connection boundary and at same level of MLFMA, thus the less empty grids are generated and higher efficiency of FFT can be obtained. While expanding basis function $\boldsymbol{f}_i$, expansion coefficient can be calculated at the coarsest level of MLFMA only and the expansion coefficient of other levels can be obtained by interpolation method.

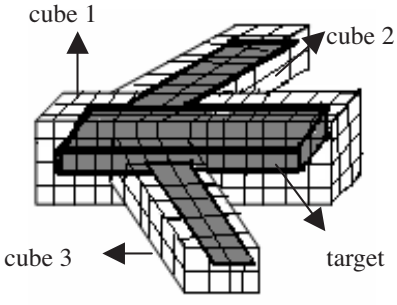

Figure 3. Target enclosed by multiple cubes.

While computing translation operator T_L, the method given by [3] is used on the base of RPFMA [4], adaptive-RPMLFMA [5] and

FAFFA-MLFMA [6], thus the T_L can be calculated on 1/8 sphere surface only and the computation complexity of MLFMA can be reduced significantly.

Using all of the improvement measures we have introduced above, the MLFMA have adaptive computation performances as follow: 1) adaptive computation of the integration of near-field interaction, $\boldsymbol{V}_{fmj}$ and $\boldsymbol{V}_{sm'i}$ by the expansion of basis function and testing function; 2) the empty grid around basis function $\boldsymbol{f}_i$ are filled adaptively and the computation of translation process meets the requirement of FFT adaptively; and 3) the precision and CPU time of the computation of T_L can be controlled adaptively. So the algorithm we presented is an adaptive algorithm.

To discrete the integral equations, the RWG basis function [7] is used for the surface of the object, and the basis function illustrated in Fig. 4(a) is used for antenna (wire), the expression of which is shown as follow.

$$\boldsymbol{f}_n^W(\boldsymbol{r}) = \begin{cases} \dfrac{\boldsymbol{\rho}_n^+}{l_n^+}, & \boldsymbol{r} \in W^+ \\ \dfrac{\boldsymbol{\rho}_n^-}{l_n^-}, & \boldsymbol{r} \in W^- \\ 0, & etl \end{cases} \tag{39}$$

The basis function illustrated in Fig. 4(b) is used to wire-surface junctions, and the expression of this kind of basis function is [8]

$$\boldsymbol{f}_n^C(\boldsymbol{r}) = \begin{cases} \boldsymbol{f}_n^{CP}(\boldsymbol{r}), & \boldsymbol{r} \in T_n^{+l} \\ \boldsymbol{f}_n^{CW}(\boldsymbol{r}), & \boldsymbol{r} \in Wire \\ 0, & etl \end{cases} \tag{40}$$

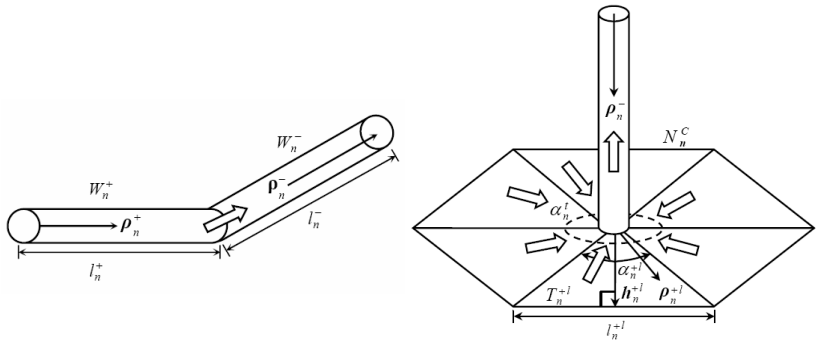

(a) (b)

Figure 4. Basis function used to wire and wire-surface joint.

where

$$\boldsymbol{f}_n^{CP}(\boldsymbol{r}) = \frac{\alpha_n^{+l}}{\alpha_n^t}\frac{1}{l_n^{+l}}\left[1 - \frac{(h_n^{+l})^2}{(\hat{h}_n^{+l}\cdot\boldsymbol{\rho}_n^{+l})^2}\right]\frac{\boldsymbol{\rho}_n^{+l}}{h_n^{+l}} \tag{41}$$

$$\boldsymbol{f}_n^{CP}(\boldsymbol{r}) = -\frac{\boldsymbol{\rho}_n^{-}}{l_n^{-}} \tag{42}$$

3. RESULTS AND DISCUSSION

In this section, the characteristics of two HF communication antennae on a ship are analyzed. The positions of these two antennae and the grid model of ship are shown in Fig. 5. The coordinates of these two antennae on the shipboard are (112.0,7.5,8.5) and (48.5,8.5,6.5). The grid model is used to obtain the geometrical data of the elements only. When we analyze this model, all the buildings on shipboard are seen as dielectric objects ($\varepsilon_r = 9.0$, $\mu_r = 1.1$) and the ship body is seen as perfect conductor (PEC). The ship dimension is about $170\times18\times6.5\,\mathrm{m}^3$ and 116796 unknowns are obtained. All the simulation process is finished on microcomputer with PIV-2.4 GHz processor and 4 GB memory.

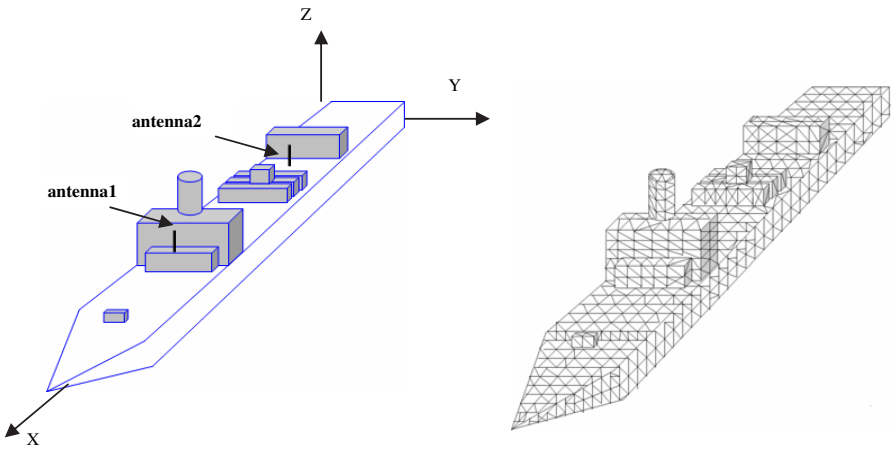

Figure 5. Model of antenna on a ship.

The radiation pattern of these two antenna in horizontal plane and vertical plane are illustrated in Fig. 6–Fig. 9. For the radiation pattern in horizontal plane, the experiment result in free space is presented first and then the experimental result on shipboard. Experiment results are

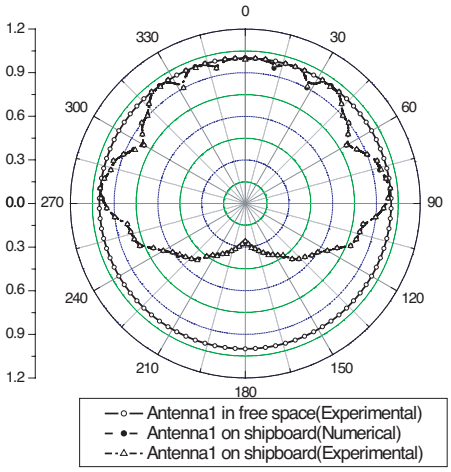

Figure 6. Radiation pattern of antenna1 (25 MHz H-H).

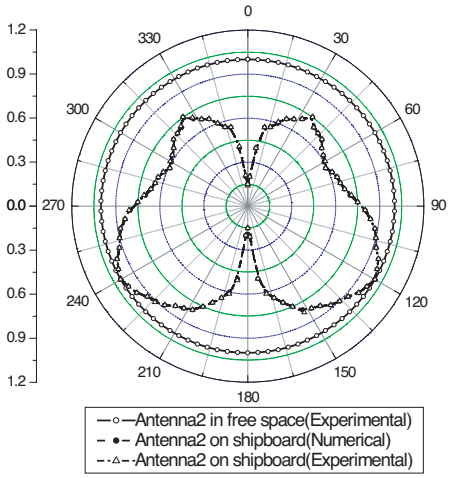

Figure 7. Radiation pattern of antenna2 (25 MHz H-H).

obtained by using a scaled ship model with the scaled ratio 1:80. We can see that radiation pattern has been modified by the effect of the ship body. The numerical result of radiation pattern in horizontal plane on shipboard is also shown in Fig. 6 and Fig. 7. The good agreement of numerical and experimental results show that the algorithm presented in this paper has very high precision. For the radiation pattern in vertical plane, only the experimental result in free space and the

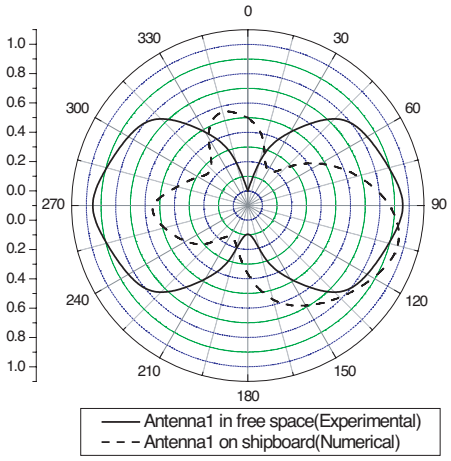

Figure 8. Radiation pattern of antenna1 (25 MHz V-V).

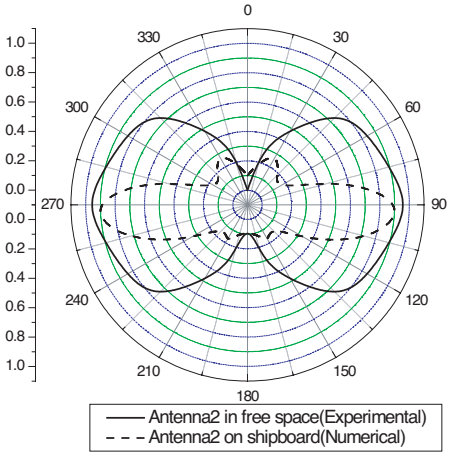

Figure 9. Radiation pattern of antenna2 (25 MHz V-V).

numerical result on shipboard are presented. The experimental result on shipboard is not given because it is very difficult to be obtained.

In Fig. 10–Fig. 12, the numerical results of the input resistance, input reactance and gain of these two antennae on shipboard are shown, where the experiment results in free space is also presented. Through both the experiment and numerical results we can see that the antenna characteristics have also been modified by the effect of the ship body.

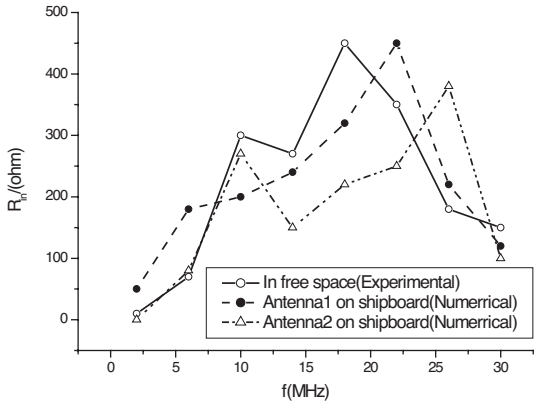

Figure 10. Input resistance of antennae.

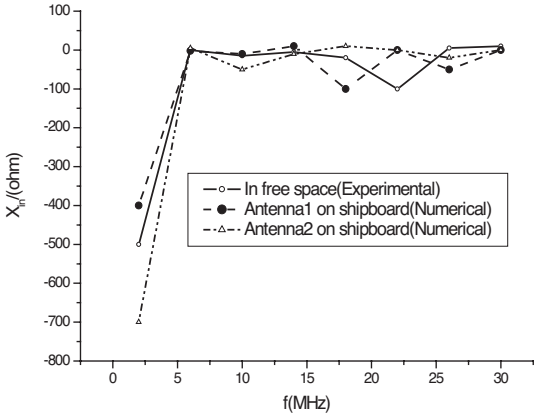

Figure 11. Input reactance of antennae.

To show the effectiveness of the adaptive MLFMA presented in this paper, we also simulated all antennae characteristics by traditional MLFMA, and the performances of them are shown in Table 1. We can see that the adaptive MLFMA has better performance than the traditional one.

Table 1. Performance of Adaptive MLFMA and MLFMA.

	Unknowns	CPU time (s)	Memory (MB)
Adaptive MLFMA	116796	139828	2659
MLFMA	116796	207669	3798

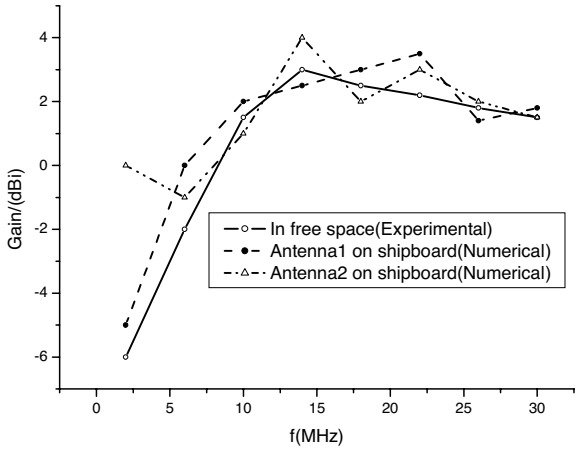

Figure 12. Gain of antennae in free space and on shipboard.

4. CONCLUSION

The computational complexity of the adaptive MLFMA presented in this paper is only about $0.7 \times O(N_s \lg N_s)$ and its memory requirement is $0.7 \times O(N_s)$, where N_s denotes the number of surface unknowns. The numerical results demonstrate that the method presented also has high precision, and the characteristics of antenna on electrically larger composite targets can be generally, accurately, efficiently computed by this technique.

REFERENCES

1. Song, J., et al., "Multilevel fast mutipole algorithm for electromagnetic scattering by large complex objects," *IEEE Trans. Antennas Propagat.*, Vol. 145, No. 10, 1488–1498, 1998.
2. Song, J. M. and W. C. Chew, "Multilevel fast multipole algorithm for solving combined field integral equations of electromagnetic scattering," *Microwave Opt. Tech. Lett.*, Vol. 10, No. 1, 14–19, 1995.
3. Wang, H.-G., Z.-P. Nie, and J. Wang, "Optimization of the invariant terms' calculation in three dimensional MLFMA," *Acta Electronica Sinica*, Vol. 28, No. 9, 105–107, 2000.
4. Wagner, R. L. and W. C. Chew, "A ray propagation fast multipole algorithm," *Microwave Opt. Tech. Lett.*, Vol. 7, No. 10, 435–438, 1994.

5. Hu, J., J. Hu, and Z.-P. Nie, "An adaptive ray-propagation multilevel fast multipole algorithm," *Chinese Journal of Radio Science*, Vol. 19, No. 6, 669–672, 2004.
6. Chew, W. C., T. J. Cui, and J. M. Song, "A FAFFA-MLFMA algorithm for electromagnetic scattering," *IEEE Trans. Antennas Propagat.*, Vol. 50, No. 11, 1641–1649, 2002.
7. Rao, S. M., D. R. Wilton, and A. W. Glisson, "Electromagnetic scattering by surfaces of arbitrary shape," *IEEE Trans. on AP*, Vol. 30, No. 3, 409–417, 1982.
8. Hwu, S. U., D. R. Wilton, and S. M. Rao, "Electromagnetic scattering and radiation by arbitrary conducting wire/surface configurations," *AP-S Digest*, Vol. 6, No. 2, 890–893, 1988.
9. Guo, J.-L., J.-Y. Li, and Q.-Z. Liu, "Analysis of arbitrarily shaped dielectric radomes using adaptive integral method based on volume integral equation," *IEEE Trans. Antennas Propagat.*, Vol. 54, No. 7, 1910–1916, 2006.
10. Zhou, B., Q. Liu, J. Guo, and Y. Ji, "Research on a sleeve antenna mounted on metallic cylinder," *Journal of Eletromagnetic Waves and Applications*, Vol. 19, No. 6, 769–777, 2005.
11. Guo, J. L., J. Y. Li, and Q. Z. Liu, "Electromagnetic analysis of coupled conducting and dielectric targets using mom with a preconditioner," *Journal of Electromagnetic Waves and Applications*, Vol. 19, No. 9, 1223–1236, 2005.
12. Zou, Y., Q. Liu, and J. Guo, "Fast analysis of body-of-revolution radomes with method of moments," *Journal of Electromagnetic Waves and Applications*, Vol. 21, No. 13, 1803–1817, 2007.
13. Zou, Y. L., J. Y. Li, and Q. Z. Liu, "Modified mode decomposition for analyzing antennas with body of revolution radome," *Journal of Electromagnetic Waves and Applications*, Vol. 21, No. 10, 1403–1410, 2007.
14. Guo, J. L., J. Y. Li, and Q. Z. Liu, "Analysis of antenna array with arbitrarily shaped radomes using fast algorithm based on VSIE," *Journal of Electromagnetic Waves and Applications*, Vol. 20, No. 10, 1399–1410, 2006.
15. Zhou, H.-J., Q.-Z. Liu, Y.-Z. Yin, and W. B. Wei, "Study of the band-notch function for swallow-tailed planar monopole antennas," *Progress In Electromagnetics Research*, PIER 77, 55–65, 2007.
16. Liu, S.-F. and S.-D. Liu, "Study on the impedance-matching technique for high-temperature superconducting microstrip antennas," *Progress In Electromagnetics Research*, PIER 77, 281–284, 2007.

17. Gupta, R. C. and S. P. Singh, "Analysis of radiation patterns of compound box-horn antenna," *Progress In Electromagnetics Research*, PIER 76, 31–44, 2007.
18. He, Q.-Q. and B.-Z. Wang, "Radiation patterns synthesis for a conformal dipole antenna array," *Progress In Electromagnetics Research*, PIER 76, 327–340, 2007.
19. Wu, Y.-J., B.-H. Sun, J.-F. Li, and Q.-Z. Liu, "Triple-band omni-directional antenna for WLAN application," *Progress In Electromagnetics Research*, PIER 76, 477–484, 2007.
20. Zhang, Y. J. and E. P. Li, "Fast multipole accelerated scattering matrix method for multiple scattering of a large number of cylinders," *Progress In Electromagnetics Research*, PIER 72, 105–126, 2007.
21. Lee, K.-C., J.-S. Ou, and C.-W. Huang, "Angular-diversity radar recognition of ships by transformation based approaches — including noise effects," *Progress In Electromagnetics Research*, PIER 72, 145–158, 2007.